Transaction B: Mechanical Engineering
Vol. 16, No. 6, pp. 525–533

Research Note

SCIENTIA IRANICA

Experimental and Numerical Investigation of Marine Propeller Cavitation

R. Arazgaldi[1], A. Hajilouy[1,*] and B. Farhanieh[1]

Abstract. *Cavitating flow is investigated around marine propellers, experimentally and numerically. Two different types of conventional model propellers are used for the study. The first one is a four bladed model propeller, so called model A, and the second one is a three bladed propeller, model B. Model A is tested in different cavitation regimes in a K23 cavitation tunnel. The results are presented in characteristic curves and related pictures. Finally, the results are discussed. Model B is investigated based on existing experimental results. In addition, model B is used for validation of the numerical solution prior to the testing of model A. The cavitation phenomenon is predicted numerically on a two dimensional hydrofoil, NACA0015, as well as propeller models A and B. The cavitation prediction on a hydrofoil is carried out in both steady and unsteady states. The results show good agreement in comparison with available experimental data. Propeller models are simulated according to cavitation tunnel conditions and comparisons are made with the experimental results, quantitatively and qualitatively. The results show good agreement with experimental data under both cavitating and noncavitating conditions. Furthermore, propeller cavitation breakdown is well reproduced in the proceeding. The overall results suggest that the present approach is a practicable tool for predicting probable cavitation on propellers during design processes.*

Keywords: *Cavitation; Marine propeller; Cavitation tunnel; Experimental; CFD.*

INTRODUCTION

Cavitation is normally defined as the formation of vapor/gas or their mixture and subsequent activities (such as growth, collapse and rebound) in liquids. Cavitation erodes machine elements, deteriorates machine performance, causes noise, vibration and even oscillation of the entire system, and also enhances corrosion/silt erosion through synergism mechanisms [1]. However, with an increasing demand for heavily loaded marine propellers, the occurrence of cavitation is inevitable nowadays. Therefore, accurate prediction of cavitation is becoming more important than ever to ensure better propulsor design [2].

Model tests provide valuable insights into cavitation physics under various predetermined conditions. However, model tests are costly and vulnerable to slight flow condition changes inside the cavitation tunnels. Moreover, it is difficult to control the inflow which is supposed to take the ship hull wake into account [2]. But, the development of new methods requires their validation against experimental results. In this paper, cavitation is simulated numerically, according to the experiments.

Computational methods for cavitation can be largely categorized into two groups: single-phase modeling with cavitation interface tracking and multi-phase modeling with an embedded cavitation interface. The former approach has been widely adopted for inviscid flow solution methods and Euler equation solvers. In [3-5], using this method, and in the framework of nonlinear cavitation theory, sheet cavitation and developed tip vortex cavitation have been simulated. In [6,7], similar methods have been used for marine propeller cavitation simulation. In [8], the Boundary Element Method (BEM) has been used for the analysis of sheet cavitation in the non-uniform wake field of marine vehicles. This method also has been developed for the investigation of partial and supercavitation on the back and face surfaces of marine propellers. Viscous-inviscid coupled formulations have also been

1. *School of Mechanical Engineering, Sharif University of Technology, Tehran, P.O. Box 14588-89694, Iran.*
*. *Corresponding author. E-mail: hajilouy@sharif.edu*

Received 23 July 2007; received in revised form 9 May 2009; accepted 1 August 2009

used for marine propeller cavitation investigation [9-11].

The latter approach can be adopted for more general viscous flow solution methods, such as the Reynolds-Averaged Navier-Stokes (RANS) equation solvers. In [12,13], using a RANS equation solver code and also using the so called "full cavitation model" by Singhal et al. [14], the cavitating flow around marine propellers in open water and vessels under wake conditions has been simulated. In [15], according to the cavitation model in [16], marine propeller thrust and torque breakdown under cavitating conditions has been investigated.

Besides theoretical methods, experimental measurements of marine propeller cavitation extension have also been carried out (e.g. [17,18]).

In this study, marine propeller cavitation is dealt with, experimentally, by investigating results from tests of propeller models in the K23 cavitation tunnel at Sharif University of Technology. The results of a model A propeller are obtained directly by the authors, whereas existing results are used for model B. Then, by solving the RANS equation and using a cavitation model, the following problems are simulated:

1. Leading edge cavitation on a hydrofoil in steady and unsteady states;
2. Open water performance of two noncavitating marine propeller models;
3. Open water performance and flow field analysis for two cavitating marine propeller models;
4. Investigation of marine propeller cavitation breakdown.

CAVITATION MODEL AND NUMERICAL METHOD

The cavitation model employed in the present study is based on the so called "full cavitation model" by Singhal et al. [14]. This model accounts for all first-order effects, i.e. phase change, bubble dynamics, turbulent pressure fluctuations and non-condensable gases. This model is under the framework of multi-phase flows and has the capability of accounting for the effects of slip velocity between liquid and gaseous phases [13].

The main part of every cavitation physical model is to find the mass transfer equation between the liquid and vapor phases which in the present study is as follows:

$$\frac{\partial}{\partial t}(\rho_m f_\nu)+\nabla.(\rho_m \overrightarrow{\nu_\nu} f_\nu)=\nabla.\left(\frac{\mu_t}{\sigma_\nu}\nabla f_\nu\right)+\mathrm{R}_e-R_c. \tag{1}$$

To solve Equation 1, R_e and R_c are to be related to the bubble dynamics and vapor volume fraction. To account for the bubble dynamics, the reduced Rayleigh-Plesset equation is employed, as for many other studies in the same modeling category. Following the approach used by Singhal et al. [14] and considering the limiting bubble size (i.e., assuming that the typical bubble diameter is the same as the maximum possible bubble size), the expressions for R_e and R_c are obtained as:

$$\mathrm{R}_e = C_e \frac{\nu_{\mathrm{ch}}}{\gamma}\rho_v\rho_l\sqrt{\frac{2}{3}\frac{p_{\mathrm{sat}}-p}{\rho_l}}(1-f_\nu), \qquad p<p_{\mathrm{sat}}, \tag{2}$$

$$\mathrm{R}_c = C_c \frac{\nu_{\mathrm{ch}}}{\gamma}\rho_l\rho_l\sqrt{\frac{2}{3}\frac{p-p_{\mathrm{sat}}}{\rho_l}}f_\nu, \qquad p>p_{\mathrm{sat}}, \tag{3}$$

where C_e and C_c are two empirical constants. Singhal et al. [14] used 0.02 and 0.01 for C_e and C_c, respectively after careful study of the numerical stability and physical behavior of the solution. Their values are adopted in the present study. The effects of turbulence induced pressure fluctuations are taken into account by raising the phase change threshold pressure from p_{sat} to p_ν, which is written as:

$$p_\nu = p_{\mathrm{sat}} + 0.5\ p'_{\mathrm{turb}}. \tag{4}$$

It is widely acknowledged that the effects of non-condensable gases need to be taken into account, as the operating liquid usually contains small finite amounts of such gases, e.g. dissolved gases and aeration. In the present model, the working fluid is assumed to be a mixture of liquid and the gaseous phases, with the gaseous phase being comprised of liquid vapor and non-condensable gas. The mixture density is calculated as:

$$\rho_m = \alpha_\nu\rho_\nu + \alpha_g\rho_g + (1-\alpha_l-\alpha_g)\rho_l. \tag{5}$$

Considering all these effects, Equations 2 and 3 can be rewritten as:

$$\mathrm{R}_e = C_e \frac{\sqrt{k}}{\gamma}\rho_\nu\rho_l\sqrt{\frac{2}{3}\frac{p_\nu-p}{\rho_l}}(1-f_\nu-f_g), \qquad p<p_\nu, \tag{6}$$

$$\mathrm{R}_c = C_c \frac{\sqrt{k}}{\gamma}\rho_l\rho_l\sqrt{\frac{2}{3}\frac{p-p_\nu}{\rho_l}}f_\nu, \qquad p>p_\nu. \tag{7}$$

The numerical study employs a cell-centered finite-volume method which allows the use of computational elements with an arbitrary polyhedral shape. Convective terms are discretized using the second-order accurate upwind scheme, while diffusive terms are discretized using the second-order accurate central differencing scheme. Velocity-pressure coupling and the overall solution procedure are based on a SIMPLE type segregated algorithm adapted to unstructured grids.

EXPERIMENTAL RESULTS

In this paper, two conventional type propeller models are used for investigation. One is the model A propeller, designed at Sharif University of Technology. The other is the model B propeller, designed at the CTO Company in Gdansk [19]. The geometries and principle particulars of the two propeller models are shown in Figure 1 and Table 1, respectively.

The K23 Cavitation Tunnel is a recirculation tunnel that has a rectangular measuring section, 650 mm wide and 350 mm deep, the length of the measuring section is 2300 mm, the contraction ratio of the nozzle is 2.45 : 1 and the height between the lower horizontal tunnel centre line and the measuring section centre line is 1482.5 mm.

The main purpose of testing the propeller models in the cavitation tunnel is determination of the characteristic curves under cavitation and non-cavitation conditions. Usually, characteristic curves are variations of thrust and torque coefficients, with respect to the advance coefficient.

In obtaining the characteristic curves, the rotational speed is kept constant and advance velocity is varied in the range of allowable cavitation tunnel flow speed (e.g., in the current cavitation tunnel, 0-3.6 m/s). Thus, different values for the advance coefficient are obtained. In the non-cavitation test, the static pressure is constant at the value of the usual operating pressure (one bar). The reasoning behind the above mentioned procedure lies in the type of dimensional analysis that is used for deriving non-dimensional coefficients in characteristic curves. In [20], the necessary dimensional analysis for open water conditions has been stated.

Table 1. Principal particular of model A and model B conventional propeller.

Model Name	Model A	Model B
Number of blades	4	3
Diameter (m)	0.29	0.153
Boss ratio	0.18	0.263
Skew (m)	0.013	0.0
Rake (m)	0.028	0.0
EAR $= A_E/A_0$	0.43	0.656

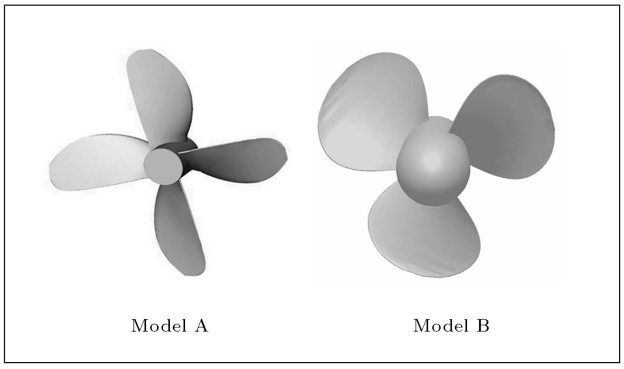

Figure 1. Geometries of model A and model B conventional propeller.

In cavitation tests, two kinds of curves are derived. One is the characteristic curve in a constant cavitation number, which is used to show the deviation of torque and thrust from a non-cavitating state. The second is the diagram of torque and thrust coefficients on the basis of the cavitation number, which is used to show the cavitation breakdown analysis. In cavitation tests, the static pressure and advance velocity inside the cavitation tunnel test section are lowered gradually in order to sketch the required diagrams.

The results of testing the model A propeller in non-cavitation states and at two rotational speeds of 700 and 900 rpm are depicted in Figure 2. Axial velocity is varied from 0.3 to 3.0 m/s. It is seen that, at low values of J, there is an appreciable difference between the results. This is a general fact because, according to the definition, K_T is proportional to the first power of thrust rather than the second power of rotational speed in the denominator. The testing of propellers for non-cavitating conditions is essential before proceeding to cavitating conditions. Firstly, using these results, the numerical method is validated for simulation of the fluid flow around the propeller models. Secondly, solving the flow fields in non-cavitating conditions is used as the initial condition for propeller cavitation simulations.

The characteristic curves in cavitation and cavitation free conditions are compared in Figure 3 for a rotational speed of 900 rpm. In the cavitation condition, the operating static pressure is reduced to 58000 Pascal in reference to the earlier inception and development of cavitation. Axial velocity is varied from 3.6 to 0.5 m/s.

For investigation of the unsteady nature of the cavitation, variation of the thrust force with respect

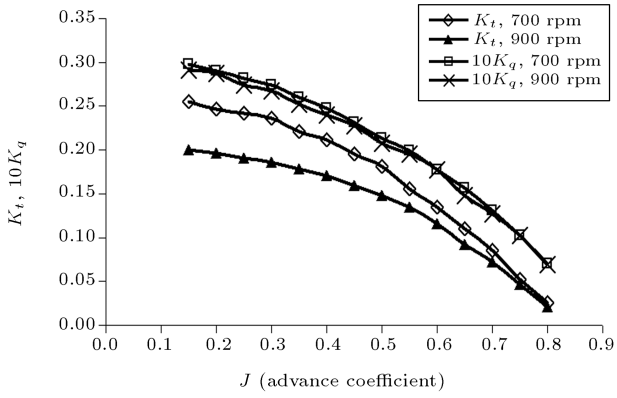

Figure 2. Characteristic curve of model A in non-cavitating state ($N = 700$ and 900 rpm).

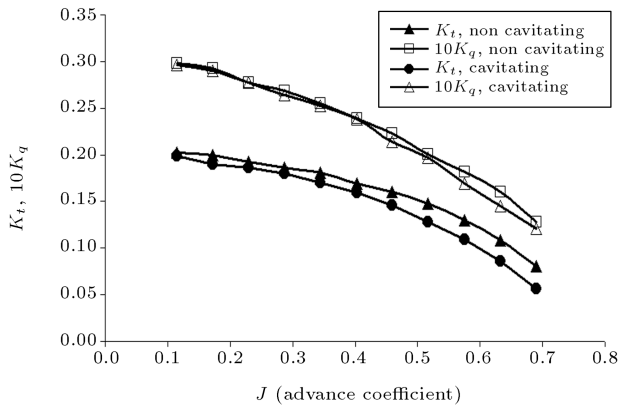

Figure 3. Comparison of characteristic curve in 900 rpm for cavitation and non-cavitation.

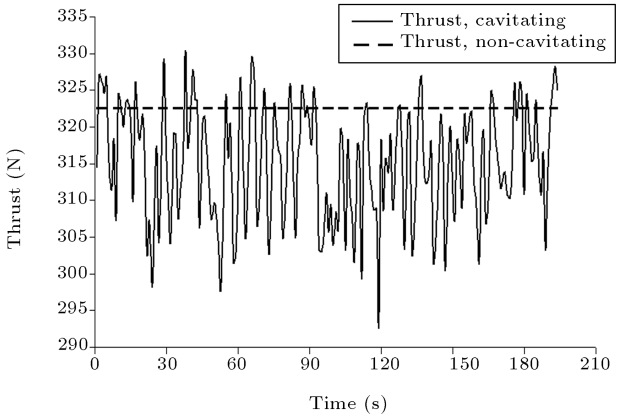

Figure 4. Thrust force unsteadiness in the cavitation condition ($N = 900$ rpm).

to time is drawn. Figure 4 shows the unsteady investigation of the cavitation at a rotational speed of 900 rpm, an axial velocity of 0.5 m/s and an operating pressure of 58000 Pascal. Thrust force oscillation is also existent in non-cavitating conditions, especially at low values of advance coefficient, and is dependent on the dynamometer load cell, free stream turbulence and larger loading on propeller blades. But, the nature of the oscillation and its amplitude difference is appreciable with respect to cavitating conditions, and the main source of oscillation in Figure 4 is the presence of unsteady cavitation.

Similar experiments are carried out at 1000 rpm. These data are used as benchmark experimental work for the present cavitation study.

The quantitative investigation of cavitation has been carried out already; and now, it is investigated qualitatively. Figure 5 shows the cavitation pictures at 900 rpm and at an axial velocity of 0.5 m/s.

The four photographs in Figure 5 are all in a one hydrodynamic condition, but the amounts of developed cavitating area are very dissimilar. In photograph A, the cavitation surface is glassy smooth and the propeller blade surface is seen clearly behind the cavitating surface. Thus, it is deduced that the formed cavitation is the sheet cavitation.

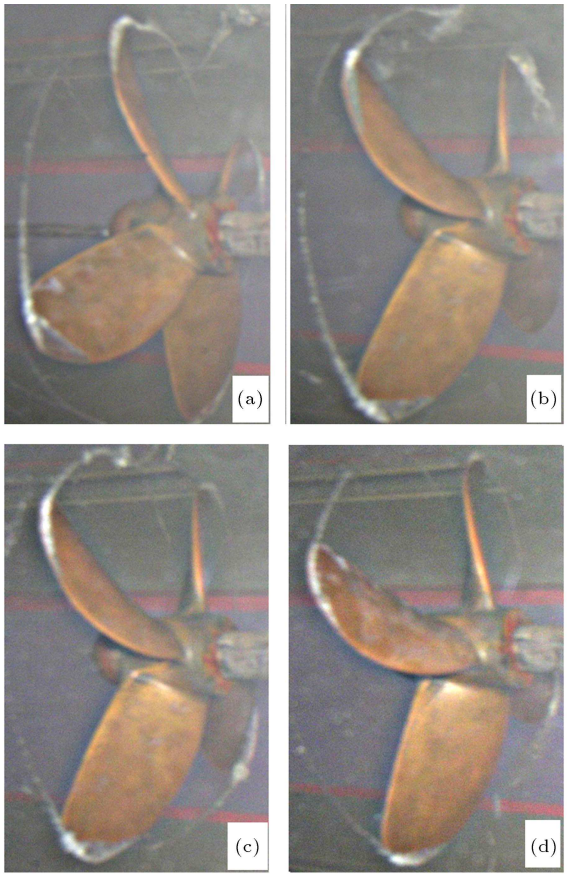

Figure 5. Illustration of propeller cavitation at rotational speed of 900 rpm and axial velocity of 0.5 m/s.

The propeller model A is also tested at 1000 rpm with similar results, but with a greater developed area. Cavitation investigation on propeller model B is carried out, only according to existing test results. The results of this model are used for validation of the numerical simulation prior to the tests of the model A propeller.

MODEL GEOMETRY AND GRID GENERATION

The leading edge cavitation on a hydrofoil is of particular interest for propeller cavitation studies, as it represents the two-dimensional characteristics of the propeller blade section. For the validation of leading edge cavitation on a hydrofoil, a NACA0015 foil section is selected. The same foil geometry was used for the experiments by Kuboto et al. [21]. A C-type grid consisting of 45,967 quadrilateral cells is generated in a computational domain. The main reason for using quadrilateral cells is the possibility of varying cell height easily in the boundary layer and is determined according to the Y^+ value. The computational domain

is determined according to the experimental setup and numerical considerations. In [21], in the perpendicular direction to the foil surface, 1.0 C, and in the downstream direction, 6.0 C, have been used. In this paper, the domain with extent $-2.5\ C \leq X \leq 4\ C$ and $-1.5\ C \leq Y \leq 1.5\ C$ is used, as shown in Figure 6.

The propeller computational domain is created as one passage surrounding the propeller where a circular cylinder with sufficient larger diameter than the propeller diameter enfolds the propeller in its cross section center and allows the fluid to pass by the model. The inlet is 1.5 D upstream; the outlet is 3.5 D downstream; solid surfaces on the blades and hub are centered at the coordinate system origin and aligned with uniform inflow; and the outer boundary is 1.4 D from the hub axis. The computational domain for propeller model A is shown in Figure 7.

The main parts of the numerical simulation of any geometry are kind, size and the meshing quality, such that their compositions severely influence convergence/divergence and the convergent time of the problem under consideration. First, the blade surface is meshed with triangles [13]. The region around the root, tip and blade edges is meshed with smaller triangles, i.e. with sides of approximately 0.003 D. The inner region is filled with triangles of approximately increased size and with aspect ratios of 1.05 and 1.1. In order to resolve the boundary layer on the solid surfaces, four layers of prismatic cells with a stretching ratio of 1.1 are grown from the blade and hub surfaces. Finally, the remaining region in the domain is filled with tetrahedral cells. Figure 8 shows the surface grids on the blade and hub surface and prismatic cells.

Because of geometry complexity, an unstructured meshing system is adopted for propellers. Also, since in 2-D simulation, unsteady simulation is carried out, for reducing the total time required, structured quadrilateral cells are used.

In order to simulate the flow around a rotating propeller, the boundary conditions are set as in the experimental setup. On the inlet boundary, velocity components are imposed for a uniform stream with a given inflow speed; on the blade and hub surface, a no-slip condition is imposed; on the lateral boundary, a slip boundary condition is imposed; and on the outlet boundary, the pressure is set to a constant value.

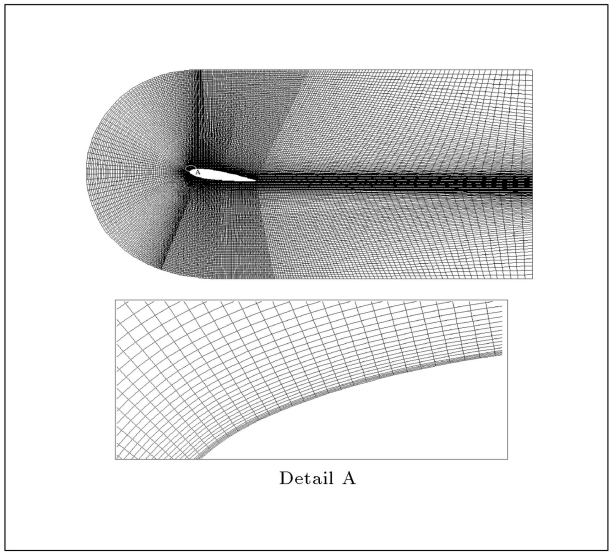

Figure 6. Computational domain and grid for leading edge hydrofoil cavitation.

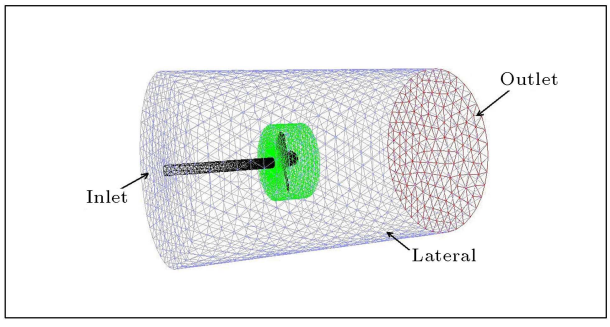

Figure 7. Computational domain for propeller model A.

NUMERICAL RESULTS EVALUATION WITH EXPERIMENTAL DATA

Cavitation on Hydrofoil

For the leading edge cavitation, the computational condition is set to the experimental one at $\alpha = 8°$, $\sigma = 1.2$ and $\mathrm{Re} = 3 \times 10^5$ [21]. Water temperature is 20°C. Figure 9 shows the vapor volume fraction contour

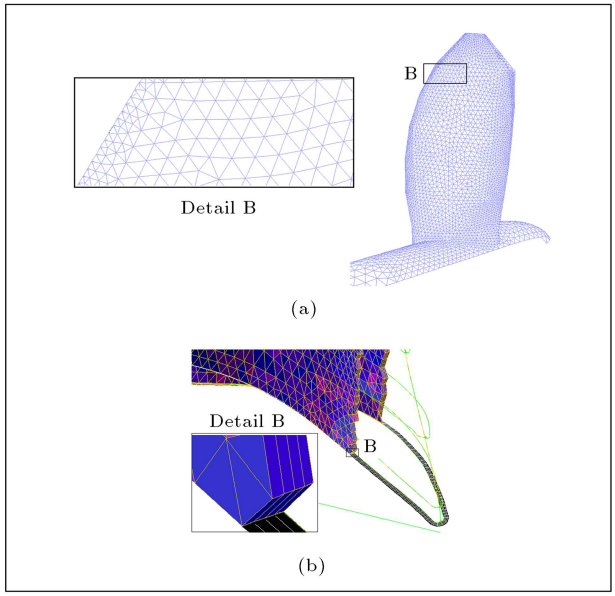

Figure 8. Surface grids for the blade (a) and hub (b) surface and prismatic cells.

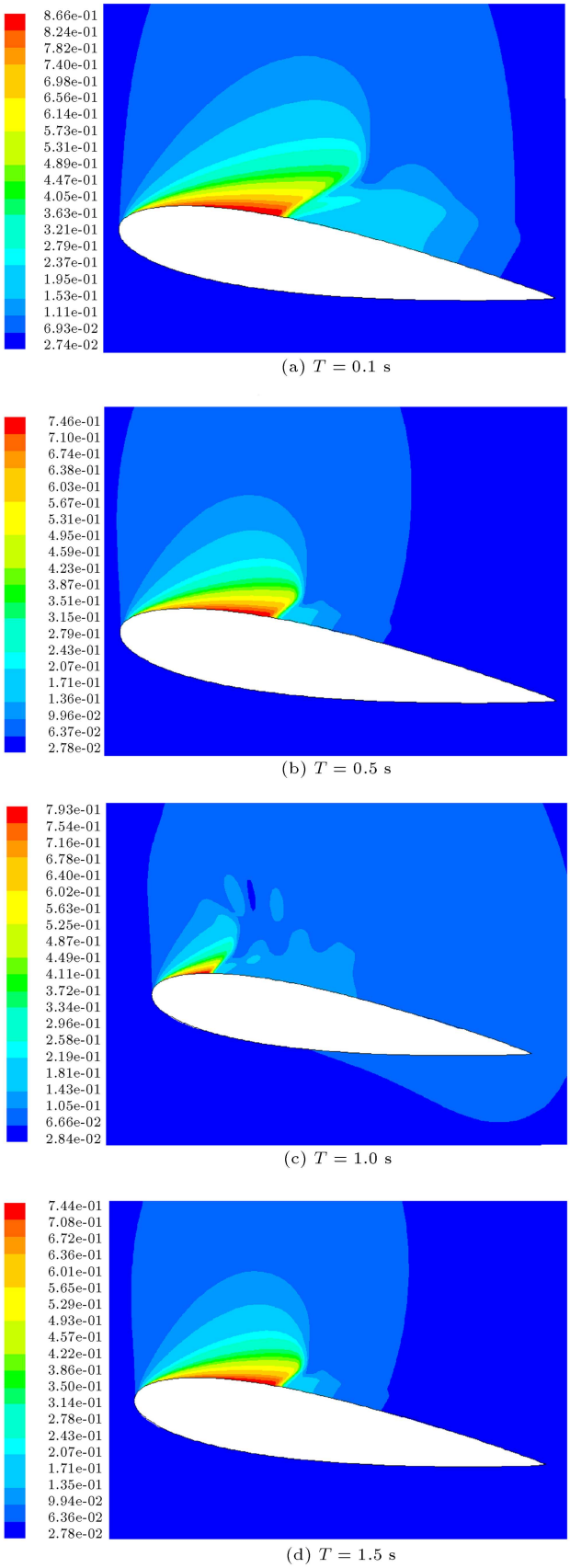

Figure 9. Vapor volume fraction distributions in cavitation number 1.2.

distribution in the experimental condition [22].

Cavitation is an unsteady phenomenon, thus the problem is solved in the unsteady state and at time duration of 7 seconds. The solution time step is 0.001 seconds and the total lasted time has been about 40 days for a PC with 3.0 GHz CPU and 1 GB of RAM. As seen from Figures 9b to 9d, it is deduced that the time period of detachment and return to initial state takes place in 1.0 seconds. The periodic behavior in the cavitation form is attributed to the existence of a vortex at the downstream end of the cavitation form and is called the re-entrant jet. This jet is propagated to the upstream under the formed cavitation, and in the vicinity of the leading edge, separates a large amount of the formed cavitation. The separated part is transported downstream by the fluid flow.

Figure 10 shows a comparison between the time-averaged pressure distribution on the foil suction and pressure surfaces and the experimental data. It shows that in the cavitating area, the pressure coefficient is approximately equal to the negative of the cavitation number (1.2). Experimental results show that there is an appreciable peak for a small length of the chord, but it is not correspondent in the numerical results. The main reason is that bubble growth in nature is a time dependent process, and at this small length of hydrofoil there is not enough time for the bubbles to reach sizes that can cause an effect on fluid flow. Also, because time averaged solutions include variable bubble lengths, this can cause some differences between results.

Also, it is deduced that the trend of C_p distribution over the back side of the profile is similar to the experimental one [22].

Figure 11 shows the comparison of pressure coefficient distribution on the foil suction side in steady state and unsteady simulation in the time period of 3-5 seconds. The pressure coefficient distribution in the two cases is nearly identical. Consequently, under operational conditions that require the investigation of

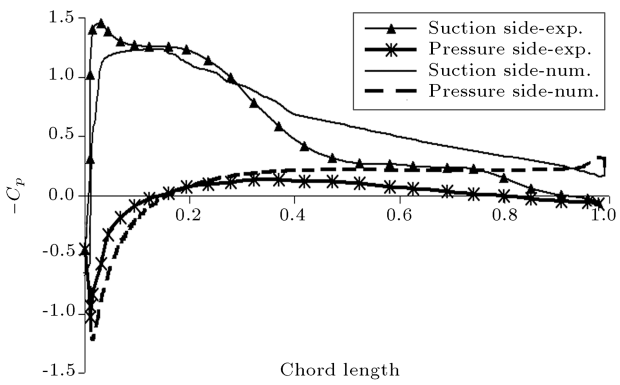

Figure 10. Time-averaged pressure coefficient comparison on suction and pressure sides.

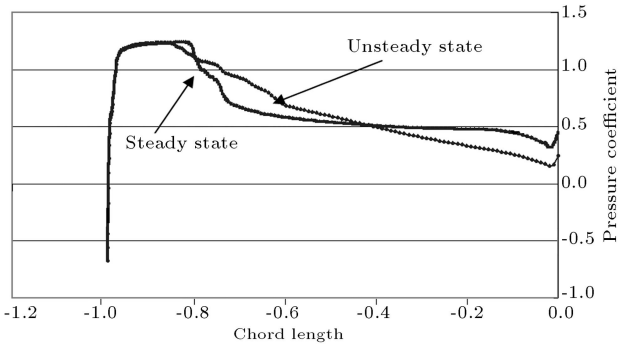

Figure 11. Comparison of pressure coefficient distribution on the steady state and time averaged condition.

lift and drag forces, steady state simulation results can be used instead of unsteady simulation [22].

Noncavitating Marine Propeller

As mentioned earlier, solving problems under noncavitating conditions is necessary before proceeding to cavitation simulations. Model A is considered in the wide range of advance coefficients, $0.1475 \leq J \leq 0.7405$, according to the variation of axial velocity from 0.5 to 2.5 m/s and the fixed value of rotational speed of 700 rpm. Figure 12 shows the characteristic curve along with the corresponding measured values for model A.

Overall, the agreement is good and trends are also well predicted. However, the CFD simulation slightly over-predicts K_q and under-predicts K_T values. According to [13], it is due to the viscous flow scale effect on the propeller performance prediction.

Cavitating Marine Propeller

Figure 13 shows a comparison of the simulated characteristic curve along with the experimental measured values for model B at a rotational speed of 2000 rpm and at an operating pressure of 0.96 atm.

Figure 14 shows the predicted characteristic values for model A along with the experimental values at a rotational speed of 900 rpm and at an operating pressure of 58000 Pascal. The data are presented for three points: a, b and c. Figure 15 shows the qualitative comparison between simulated and experimental ones in point A of Figure 14. As mentioned earlier, the numerical simulation in the steady state must be compared with the time averaged value of the experimental results.

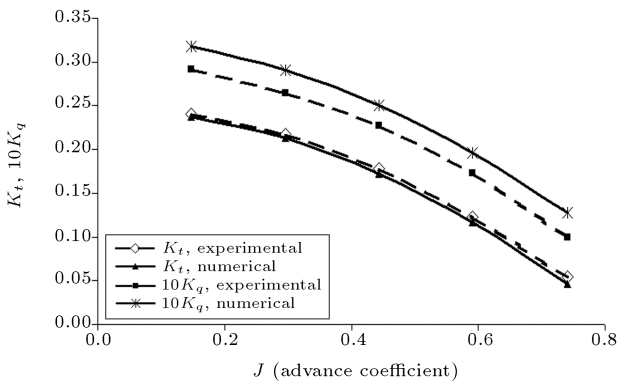

Figure 12. Characteristic curves at non-cavitating conditions for model A.

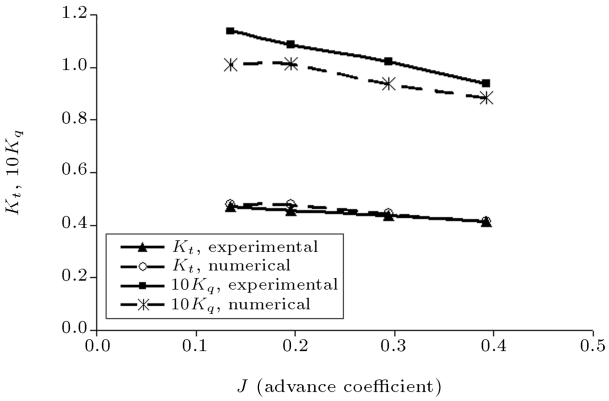

Figure 13. Comparison of characteristic curve for model B.

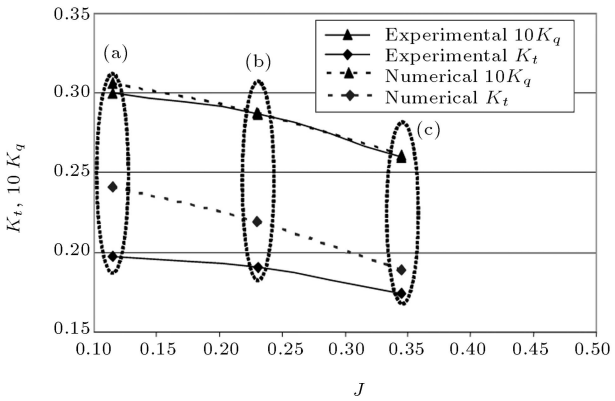

Figure 14. Characteristic curves for model A in 900 rpm.

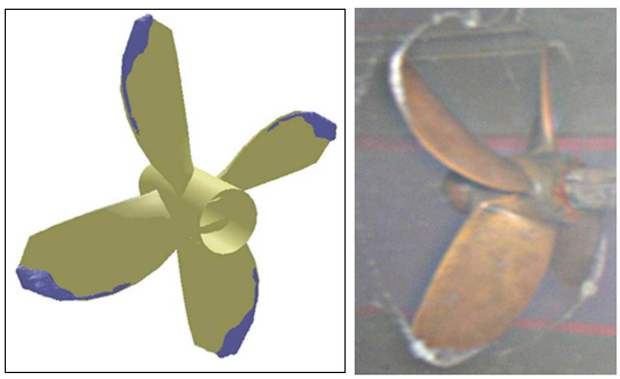

Figure 15. Cavity shape on the blade; (a) Simulation; (b) Experiment.

The next problem is the numerical simulation of the tip vortex cavitation. As seen in Figure 15, the simulation shows an abrupt termination right behind the tip and the vortex cavity is missing. In [12,13], the disability of the current cavitation simulation is attributed to insufficient grid resolution, but the authors believe that it is mainly attributed to the cavitation model itself, which only considers bubble growth in the low pressure region and, then, to its disappearance in the high pressure region. The next reason can be due to the steady state simulation of the phenomena. However, as shown in the hydrofoil case, the chance of this reason is weak.

One of the major issues in cavitating marine propellers is the breakdown of the thrust and torque. Figure 16 presents the K_T and K_q versus σ_{rot} at advance coefficients of $J = 0.23$ and $J = 0.172$, while at $J = 0.172$, i.e. at high load and large angle of attack, higher breakdown is observed with respect to $J = 0.23$ at the specified cavitation number.

Figure 17 shows cavitation development at $J = 0.172$ and $\sigma_{\text{rot}} = 0.2522$, which corresponds to the cavitation breakdown. It is observed that K_T and K_q start decreasing when one third of the blade upper surface is occupied by cavitation development.

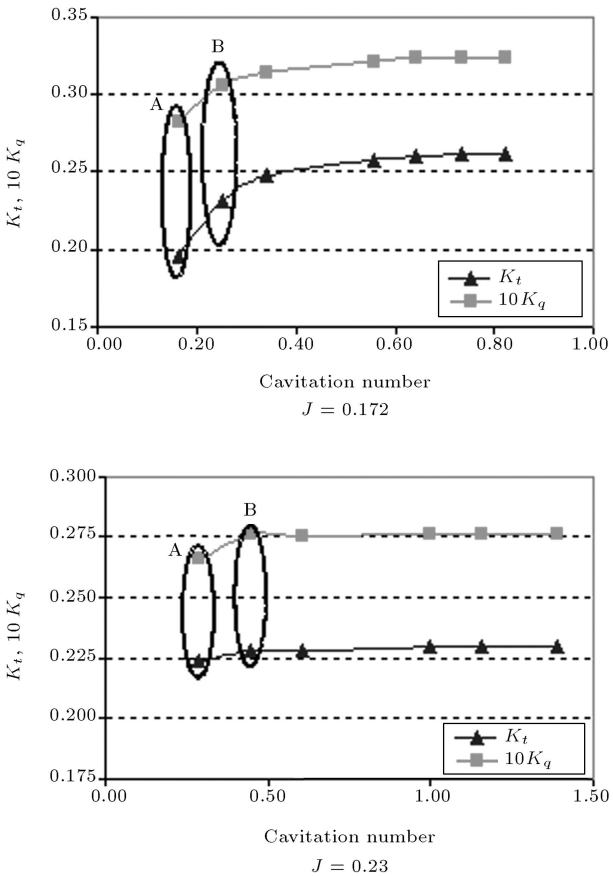

Figure 16. K_t and K_q versus σ_{rot} at advance coefficients of $J = 0.23$ and $J = 0.172$.

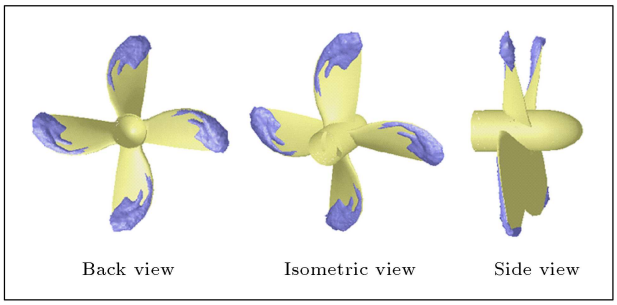

Figure 17. Cavitation development on blades at $J = 0.172$ and $\sigma_{\text{rot}} = 0.2522$.

CONCLUSION

In this paper, cavitating flow is investigated experimentally on two conventional marine propellers. In the numerical simulation, cavitating flow is simulated on a two-dimensional hydrofoil and two conventional marine propellers. Simulations are carried out according to the "full cavitation model" by Singhal et al. [14].

Validation of the hydrofoil simulation is carried out according to existing experimental data and the results show comparatively good conformity. Validating the propellers is performed under a wide range of advance coefficients and cavitation numbers, according to the cavitation tunnel results. In cavitating propeller cases, predicted global quantities, such as thrust and torque are in good agreement with measured values. Cavitation breakdown is also investigated as one of the major results of cavitation appearance.

Model B showed lower cavitation extension rather than model A, because of its greater EAR. Also, leading edge cavitation started earlier in this model than in model A.

The overall results show that the present simulation method is applicable to actual cavitating propeller design procedures.

ACKNOWLEDGMENT

The authors would like to thank Dr. M.S. Seif, head of the Marine Laboratory at Sharif University of Technology for his kind cooperation. The helpful suggestions of Eng. M. Askari and Eng. V. Alizadeh are also gratefully acknowledged.

NOMENCLATURE

f_g, f_ν	gas and vapor mass fraction
V_ν	vapor phase velocity (m/s)
R_e, R_c	rate of vapor generation and condensation
p_{sat}	liquid saturated pressure (Pascal)
p	flow field static pressure (Pascal)

$k_T = \frac{\text{thrust}}{\rho N^2 D^4}$	thrust coefficient
ρ_m, ρ_ν, ρ_l	mixture, vapor and liquid density
μ_t	turbulent eddy viscosity
V_{ch}	characteristics speed
$J = \frac{V_A}{ND}$	advance coefficient
V_A	inflow speed (m/s)
k	local turbulent kinetic energy
p'_{turb}	turbulence-induced pressure fluctuations
D	propeller diameter (m)
N	propeller rotational speed
$k_q = \frac{\text{torque}}{\rho N^2 D^5}$	torque coefficient
$\alpha_\nu, \alpha_g, \alpha_l$	vapor, gas and liquid volume fraction
σ_ν	turbulent Prandtl number
$\sigma_{\text{rot}} = \frac{P - P_{\text{sat}}}{\frac{1}{2}\rho((\pi N D)^2 + V_A^2)}$	rotational cavitation number
σ	hydrofoil cavitation number
C	hydrofoil chord length

REFERENCES

1. Li, S.C., *Cavitation of Hydraulic Machinery*, University of Warwick, Imperial College Press, UK (2000).
2. Rhee, S.H. et al. "Propeller cavitation study using an unstructured grid based Navier-Stokes solver", *ASME J. Fluids Eng.*, **127**, pp. 986-994 (2005).
3. Kinnas, S.A., Lee, H. and Young, Y. Lu. "Boundary element techniques for the prediction of sheet and developed tip vortex cavitation", *Electronic Journal of Boundary Elements*, **BETEQ2001**(2), pp. 151-178 (2002).
4. Kinnas, S.A., Lee, H. and Young, Y. Lu. "Modeling of unsteady sheet cavitation on marine propeller blades", *International Journal of Rotating Machinery*, **9**, Taylor & Francis Inc., pp. 263–277 (2003).
5. Lee, H. and Kinnas, S.A. "Application of BEM in unsteady blade sheet and developed tip vortex cavitation prediction on marine propellers", *IABEM 2002, International Association for Boundary Element Methods*, UT Austin, TX, USA (May 28-30 2002).
6. Ghassemi, H. "Boundary element method applied to the cavitating hydrofoil and marine propeller", *Scientia Iranica*, **10**(2), pp. 142-152 (2003).
7. Salvatore, F., Pereira, F. and Felice, F. Di. "Numerical investigation of the cavitation pattern on a marine propeller: Validation vs. experiments", *A Report of INSEAN Research Program*, Rome, Italy (2000-02).
8. Young, Y.L. and Kinnas, S.A. "A BEM for the prediction of unsteady midchord face and-or back propeller cavitation", *ASME J. Fluids Eng.*, **123**, pp. 311-319 (2001).
9. Krasilnikov, V.I. and Berg, A. "Numerical prediction of sheet cavitation on rudder and podded propellers using potential and viscous flow solutions", *Proc. of the 5th Int. Symposium on Cavitation - CAV'2003*, Osaka, Japan (Nov. 1-4, 2003).
10. Salvatore, F., Testa, C. and Greco, L. "A viscous-inviscid coupled formulation for unsteady sheet cavitation modeling of marine propellers", *5th Int. Symposium on Cavitation (CAV2003)*, Osaka, Japan (Nov. 1-4, 2003).
11. Chahine, G.L. and Hsiao, C.T. "Numerical investigation of sheet and cloud cavitation inception and dynamics on propeller blades", *DYNAFLOW. Inc, Report 97001-1* (2001).
12. Watanabe, T., Kawamura, T., Takekoshi, Y., Maeda, M. and Rhee, S.H. "Simulation of steady and unsteady cavitation on a marine propeller using a RANS CFD code", *Fifth International Symposium on Cavitation (Cav2003) Osaka*, Japan (Nov. 1-4, 2003).
13. Rhee, S.H., Kawamura, T. and Li, H. "Propeller cavitation study using an unstructured grid based Navier-Stoker solver", *ASME J. Fluids Eng.*, **127**, pp. 986-994 (2005).
14. Singhal, A.K., Athavale, M.M., Li, H. and Jiang, Y. "Mathematical basis and validation of the full cavitation model", *ASME J. Fluids Eng.*, **124**, pp. 617-624 (2002).
15. Lindau, J.W., Boger, D.A., Medvitz, R.B. and Kunz, R.F. "Propeller cavitation breakdown analysis", *ASME J. Fluids Eng.*, **127**, pp. 995-1002 (2005).
16. Kunz, R.F. et al. "A preconditioned Navier-Stokes method for two-phase flows with application to cavitation prediction", *PERGAMON Journals, Computers & Fluids*, **29**, pp. 849-875 (2000).
17. Pereira, F., Salvatore, F. and Felice, F.D. "Measurement and modeling of propeller cavitation in uniform inflow", *ASME J. Fluids Eng.*, **126**, pp. 671-679 (2004).
18. Pereira, F., Salvatore, F., Felice, F.D. and Elefante, M. "Experimental and numerical investigation of the cavitation pattern on a marine propeller", *24th Symposium on Naval Hydrodynamics*, Fukuoda, Japan (July 8-13, 2002).
19. "Propeller model no. P84", CTO Co., Gdansk, Poland (1978).
20. Carlton, J.S., *Marine Propeller and Propulsion*, Butterworth-Heinemann Ltd (1994).
21. Kuboto, A., Kato, H. and Yamaguchi, H. "A new modeling of cavitating flows: a numerical study of unsteady cavitation on a hydrofoil section", *ASME J. Fluids Eng.*, **240**, pp. 59-96 (1992).
22. Arazgaldi, R. "Experimental and theoretical investigation of marine propeller cavitation", Master of Science Thesis, Sharif University of Technology, Tehran, Iran (Dec. 2006).